Journal of Membrane Science 597 (2020) 117619

Contents lists available at ScienceDirect

Journal of Membrane Science

journal homepage: http://www.elsevier.com/locate/memsci

Particle counting and tracking: Zooming on deposition and flow paths during initial stages of cake formation in forward osmosis with spacers

Anne Bogler [a,1], Andreas Kastl [b,1], Markus Spinnler [b], Thomas Sattelmayer [b], Avraham Be'er [a], Edo Bar-Zeev [a,*]

[a] Zuckerberg Institute for Water Research (ZIWR), The Jacob Blaustein Institutes for Desert Research (BIDR), Ben-Gurion University of the Negev, Sede Boqer Campus, 84990, Israel

[b] Lehrstuhl für Thermodynamik, Technische Universität München, Boltzmannstr. 15, 85748, Garching, Germany

ARTICLE INFO

Keywords:
Particle tracking
Forward osmosis
Spacer
Biofouling
Bacteria
Beads

ABSTRACT

Deposition and flow paths of particles (live and inert) often control the first stages of "cake" (fouling) formation in membrane systems. Developments in crossflow cell design such as three-dimensional (3D) printing and state of the art imaging techniques enable *real-time* and *in situ* tracking of initial cake formation. In this work, high-resolution large-field fluorescent microscopy was used to concomitantly study and compare the deposition and flow paths of inert beads and *Bacillus subtilis* as biofilm forming bacteria. The membrane surface was imaged continuously (30 s intervals) during the initial stages of cake formation (< 4 h) in a 3D printed forward osmosis (FO) cell containing diamond-shaped spacers. Deposition patterns were analyzed using particle detection and counting for quantitative comparison. Flow paths and velocities (< 17 μm s^{-1}) of beads were similar to those of *B. subtilis*, thus providing a reliable approximation for bacteria passing through the feed channel. However, spatiotemporal deposition of beads and bacteria were markedly different: Final bacteria deposition was 20 times lower than that of beads when normalized to the initial foulant concentration in the feed solution, although beads had a linear deposition increase, while bacteria deposition rose exponentially. Additionally, deposition of beads was homogeneously distributed within the spacer element compared to bacteria, which were mostly captured around the spacer filaments obstructing the flow. Our results provide a novel approach to quantify cake formation in membrane systems as well as new insights on the impact of inert and living particles on the deposition patterns and flow paths during the first stages of cake formation. These insights could be applicable to design new membrane surfaces and spacer shapes that minimize and delay fouling development.

1. Introduction

Wastewater treatment for recycling and reuse with membrane technologies, such as forward osmosis (FO), has been gaining interest due to increasing water scarcity [1,2]. FO technology utilizes an osmotic pressure gradient between a dilute feed solution and a concentrated draw solution on the opposing sides of a semipermeable thin-film composite membrane. The osmotic pressure gradient causes pure water to cross the FO membrane from the feed to the draw solution, while contaminants are rejected [3,4]. FO spiral wound modules comprise multiple membrane flat sheets that are wound around a central tube and are separated by channel spacers [5,6]. Contaminants in wastewater often contain high concentrations of bacteria and organic material that result in the formation of a foulant "cake" with severe consequences for system performance [7,8]. Cake formation (*e.g.*, biofilm in the case of bacteria) commences immediately upon contact with wastewater as the first contaminants, such as bacteria, are deposited on the membrane surface and feed channel spacers. Progression of cake or biofilm formation ultimately leads to feed channel blockage and reduction in permeate water flux via cake enhanced concentration polarization [9,10]. We surmise that it is imperative to understand the factors governing the deposition patterns during the initial stages of cake formation to tackle future biofouling mitigation approaches.

Deposition of bacteria in membrane systems has previously been

* Corresponding author.
E-mail addresses: bogler@post.bgu.ac.il (A. Bogler), kastl@td.mw.tum.de (A. Kastl), spinnler@td.mw.tum.de (M. Spinnler), sattelmayer@td.mw.tum.de (T. Sattelmayer), beera@bgu.ac.il (A. Be'er), barzeeve@bgu.ac.il (E. Bar-Zeev).
[1] These authors contributed equally.

https://doi.org/10.1016/j.memsci.2019.117619
Received 30 August 2019; Received in revised form 10 October 2019; Accepted 26 October 2019
Available online 28 October 2019

studied using a variety of *in situ* microscopic approaches [11–13]. However, simple channel geometries without spacers were mostly applied, and inert beads were often used as an approximation for bacteria [11,14,15]. Instead, studies using bacteria as a foulant for *in situ* observation of biofilm formation often focused on the later stages of biofilm development [16–18]. To date, different spacer configurations have been investigated by qualitatively comparing deposition patterns and modeling trajectories of depositing beads during the first hours of foulant accumulation [14,15]. Additional insights can be gained by quantifying deposition patterns with image analysis for the detection and counting of particles on the membrane surface. Concomitantly, particle detection can also be applied to follow depositing foulants using particle tracking [19,20]. Image sequences of *in situ* observations can be analyzed by detecting single particles in each image, then assigning them to their new position in the subsequent images to obtain specific flow paths towards the membrane surface [19,20]. *In situ* observations that are required for such analyses have been facilitated by new flow cell designs and production methods, such as 3D printing [21]. These new flow cells can be printed from a wide range of materials, from transparent plastic to aluminum and even steel. This diversity allows printing of a complete cell configuration with fine details and sufficient strength to withstand pressure where needed. Compiling 3D printed flow cells for direct *in situ* tracking and quantifying the initial deposition of different foulants may provide new insights for biofouling mitigation approaches [22–24].

This study investigated the flow paths and initial deposition of inert beads and bacteria during the first stages of cake formation in forward osmosis using a specifically designed flow cell for *in situ* tracking and image analysis. Images captured by high-resolution large-field fluorescence microscopy were analyzed quantitatively for spatiotemporal deposition patterns as well as flow paths by particle counting and tracking. The methods were adapted for the analysis of two types of particles, namely inert polystyrene beads (1 μm) and fluorescently tagged *Bacillus subtilis* bacteria. Our results highlight the advantages and limitations of using beads for the approximation of the first critical stages of biofilm formation.

2. Materials and methods

2.1. Experimental FO system

Initial accumulation of particles (*i.e.,* beads or bacteria) was determined in a bench-scale FO membrane system comprising a 3D printed membrane crossflow cell (Fig. 1 A and B). The flow cell was placed under a large-field epifluorescent microscope for direct *in situ* and *real-time* observation of fluorescent beads and bacteria that passed through the feed channel. The FO system was operated in a closed-loop mode and solution temperatures were held constant at 25 ± 0.5 °C. The crossflow was generated by small centrifugal pumps (Atman, China), adjusted with needle valves (Ham-Let, Israel) to reach a crossflow velocity of 1 cm s^{-1}, and controlled by volumetric measurements. Compared to commonly used values (~10 cm s^{-1}), the crossflow velocity was reduced significantly to expedite deposition and enhance differences between foulant types [5,25–28]. The feed reservoir was placed on a stirrer to avoid foulant deposition.

2.2. 3D printed membrane crossflow cell

Direct observation of the feed channel was facilitated by a specifically designed 3D printed membrane crossflow cell (Shapeways, USA, Figures S1 – S5) with a viewing window on the feed side (Fig. 1 C). To date, a wide range of materials is available for 3D printing and the best material for each part of the crossflow cell can be chosen. Thus, the two cell halves were printed using an acrylic photopolymer (Visijet® M3 Crystal, 3D Systems, USA). The material proved suitable and durable, with leak free and satisfactory performance throughout the study. A 60% stainless steel, 40% bronze matrix material (420 stainless steel infiltrated with bronze, ExOne, USA) was chosen for the support plates in order to give sufficient strength for the complete closure of the cell. A microscope slide (Menzel, Thermo Fisher, USA) was glued into the feed cell half as the viewing window to facilitate optimal optical access. The choice of the materials in addition to the high resolution and manufacturing speed of the 3D printing method makes it possible to easily redesign and fit the flow cell for applications in membrane distillation or pressure driven systems [29–31]. O-rings were placed in the cell halves to seal the channels and define the membrane area (7.9 × 3.7 cm^2). A commercial thin-film composite FO membrane (FOMEM-0415, Porifera, USA) was held between the feed and draw spacers (17 mils = 0.43 mm, Conwed®, USA). Spacers were oriented in a diamond-shaped pattern and comprised polypropylene filaments. Additional details on the 3D printed flow cell can be found in the supporting information.

2.3. Bacterial strain and growth protocol

A genetically modified fluorescent strain of *Bacillus subtilis* (wild type strain 3610) was used for biofouling experiments. *B. subtilis* is a rod-shaped (0.8 μm × 5 μm), Gram-positive and motile bacteria that can often be found in different types of wastewater [12,32,33]. As such, *B. subtilis* has frequently been used as a model bacterial species for a

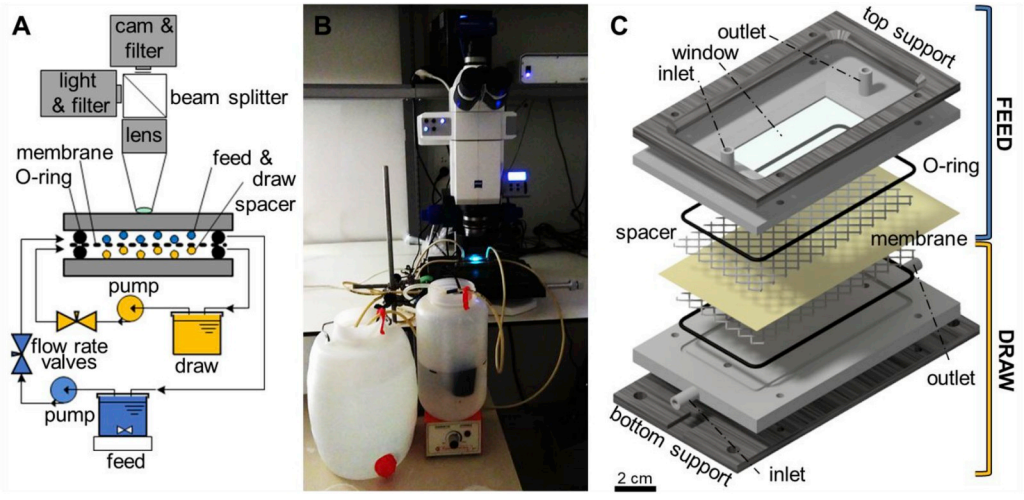

Fig. 1. Schematic description of the experimental system. (A) Schematic drawing of the bench-scale FO system with a cross-sectional view of the membrane crossflow cell, including spacers. (B) Photograph of the experimental system with feed and draw reservoirs as well as the flow cell placed under the epifluorescent microscope. (C) Exploded view of the 3D printed flow cell and the components inside the membrane channels. The components are mirrored at the membrane with a spacer, O-ring, cell half (comprising inlet and outlet) and a support plate on each side.

wide range of bacterial studies [34–36]. *B. subtilis* cells have been determined to be highly hydrophilic (contact angle of 21°) and possess a negatively charged cell surface [12]. Previously, *B. subtilis* was genetically labeled with a green (ex. 470 nm, em. 525 nm) fluorescent protein, which enabled cell visualization in *real-time*. In this study, *B. subtilis* was first grown overnight (8–12 h) in Luria–Bertani broth (LB, Becton, Dickinson and Company). Bacteria were then diluted and regrown for an additional 1–2 h to a mid-exponential state (OD_{600} of 0.5). LB was removed by centrifugation at 4000 rpm for 20 min and the bacteria were re-suspended in sterile artificial secondary effluent wastewater [37]. Due to the low exposure time (240 s during 4 h) of bacteria to light, photo bleaching effects were avoided during the experiments. The bacterial suspension was diluted by the feed solution to a concentration that is representative of secondary wastewater effluent composition ($1.9 \pm 0.46 \times 10^9$ cells L^{-1}) [38,39].

2.4. Fluorescent beads

FluoSpheres® carboxylate-modified microspheres (Molecular Probes, USA) with a diameter of 1 μm were used as inert particulate foulant. The beads are made of polystyrene and coated with a polymer that comprises several carboxylic acids, resulting in a hydrophilic, negatively charged surface [40]. These beads were loaded with a dye for orange fluorescence (ex. 540 nm, em. 560 nm), which was embedded internally with a negligible effect on surface properties and minimal photo bleaching [40]. The stock was diluted by 10^3 before it was added to the feed solution with a further dilution of 10^3, which resulted in a concentration of $3.6 \pm 0.32 \times 10^7$ beads L^{-1}. Due to the strong fluorescence of the beads, the concentration had to be reduced as compared to the bacteria, such that the initial deposition of single particles could be observed over a similar time frame (4 h) for both foulant types.

2.5. Experimental procedure

Each experiment was initiated by adding sterile artificial secondary effluent wastewater (2 L) to the feed reservoir [41,42]. The wastewater contained a carbon source in the form of sodium citrate (0.6 mM $Na_3C_6H_5O_7$) and glucose (2.7 mM $C_6H_{12}O_6$) in biofouling experiments. Concomitantly, the concentration of the draw solution (8 L) was adjusted to approximately 1 M NaCl with a 5 M stock solution to reach a permeate water flux of 27 ± 2.9 L m^{-2} h^{-1}, which is within the range of permeate water flux in operational FO systems [43,44]. The solutions were allowed to mix for approximately 15 min before fluorescent beads or *B. subtilis* were added to the feed wastewater. Image acquisition was initiated directly after foulant addition. Feed subsamples were taken every 60 min for analysis of foulant concentration with an Attune NxT flow cytometer (life technologies, Thermo Fisher Scientific, USA, Fig. S6). Flow paths and deposition patterns were imaged in three individual experiments for each foulant. Additional details on wastewater composition, beads, and bacterial abundance, as well as the flow cytometry analysis, are given in the supporting information.

2.6. Image acquisition

Images were obtained via the program ZEN 2.6 (Zeiss, Germany) and an epifluorescent microscope (Axio Zoom, V16, Zeiss, Germany) equipped with a PanNeoFluar objective and an Axiocam 506 mono camera. Detailed description of the microscope properties and image acquisition can be found in the supporting information (Table S1). Images of one spacer element ($\sim 1.5 \times 1.5$ mm^2) were captured every 30 s for deposition over time (4 h) at 20× magnification and with the focus on the membrane surface (<40 μm). Movies of 30 s duration were taken at the beginning of each experiment for particle tracking with a magnification of 60×, which reduced the focus depth (<7 μm) as well as the field of view and necessitated imaging of five locations within the spacer element (Fig. S7).

2.7. Image analysis: particle detection and tracking

Recorded movies were exported from ZEN as sequences of single-frame images and analyzed in MATLAB® (The Mathworks™, Inc.). The diamond-shaped membrane area enclosed by one spacer element was analyzed with the procedure depicted in Fig. 2, while the area lying beneath spacer filaments and outside of the observed spacer element was omitted. A detailed explanation of the image analysis procedure and validation (Fig. S8) can be found in the supporting information.

2.8. Statistical analysis

All statistical analyses were performed with the Excel add-in XLSTAT (Addinsoft, USA). As a first step for the analysis of particle deposition, exponential smoothing was performed on the time series to reduce artifacts in particle numbers due to flickering. Statistically significant differences were determined with the analysis of variance (ANOVA) at a significance level of $p < 0.05$ and post hoc multiple comparison methods of Tukey HSD, Fisher LSD, and Newman-Keul's (SNK).

3. Results and discussion

3.1. Spatiotemporally resolved quantification of deposition and flow paths by high resolution, large-field fluorescence microscopy

Fluorescence microscopy with a high resolution and a large field of view was used to quantify foulant deposition as well as to determine flow paths in this study. Resolving single particles in fluorescence microscopy is not directly related to the magnification, but is rather a function of the light emitted from the excited particles. This approach enables capturing two-dimensional information of a whole spacer element in one image, while still distinguishing between single particles with a diameter even smaller than 1 μm. Due to the black background given by the non-fluorescent membrane, quantification of deposition by detecting single fluorescent particles is simpler compared to conventional bright-field microscopy. Image series with arbitrary time intervals can thus be analyzed efficiently. However, particles need to be fluorescent, and quantification is limited to the initial stages of cake formation, as multiple layers cannot be distinguished. Over time, when complex multilayers form, other techniques including confocal laser scanning microscopy (CLSM) and optical coherence tomography (OCT) come into play, as both can resolve the foulant cake in three dimensions. However, CLSM is limited regarding the size of the field of view, as well as frame rate to values that only allow tracking at very low crossflow velocities [36] compared to 2D fluorescence microscopy. On the other hand, OCT is more applicable at the mesoscale, namely capturing larger biofilms (10 – 1000 μm) [17,45] over longer durations than 4 h [16–18], and can therefore not be used to image the initial stage of biofilm formation or track the movement of single cells.

Calculation of flow paths with particle tracking was obtained in this study with the same setup, while quantifying foulant deposition. This simplifies the investigation of the cake effects on the flow path within the ongoing experiment using the different foulants. Particle imaging velocimetry (PIV) is similar to particle tracking and a well-established method. Although used in a few membrane studies to quantify fluid flows in spacer filled channels, PIV requires high frame rates as well as high particle concentrations, which would impede simultaneous deposition quantification [25,46,47]. Similarly, other methods for flow quantification would require expensive additional setups that are unable to simultaneously capture deposition [48–50]. Following the above, using large-field fluorescent microscopy enables concomitant determination of foulant deposition and flow paths with high resolution over time and space as well as efficient analysis.

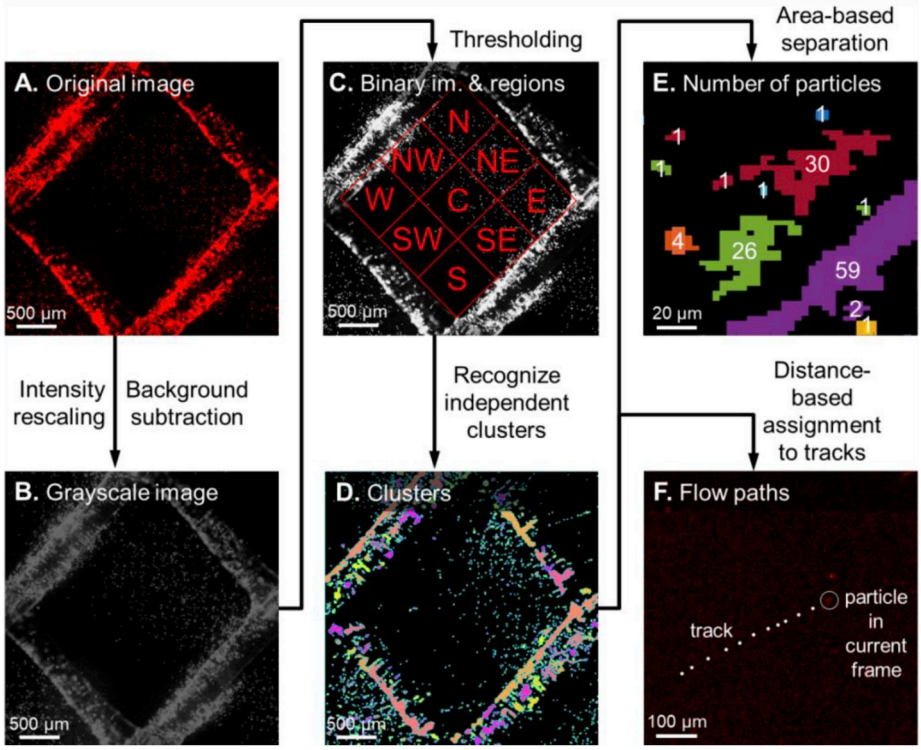

Fig. 2. Image analysis procedure used to determine particle deposition and flow paths, with example images for each step. The original image (A) was preprocessed by background subtraction, intensity rescaling (B), and thresholding (C). The membrane area within the spacer element was separated into 9 regions, named according to the cardinal directions (C). Beads and bacteria were counted by first identifying independent clusters of high intensity (D). Then the number of particles contained in each cluster was calculated by assuming that one particle is represented by five pixels (E). Flow paths were obtained by assigning particles of the current frame to tracks from the previous frames (F).

3.2. *Flow paths and particle velocities near the membrane surface during initial cake formation*

Crossflow direction and spacer geometry determine the paths that particles follow through a feed channel [25,51]. Particles with a similar density as water (e.g. beads and bacteria) are assumed to move with the surrounding fluid and can thus give insights into the velocity and direction of the fluid flow [19,20]. Similar to industrial membrane modules, spacer orientation in this study formed a 45° angle between the flow direction and spacer filaments (Fig. 3 A). In this configuration, filaments I and III are in contact with the glass, while II and IV are in contact with the membrane. Due to the irregular shape of the spacer

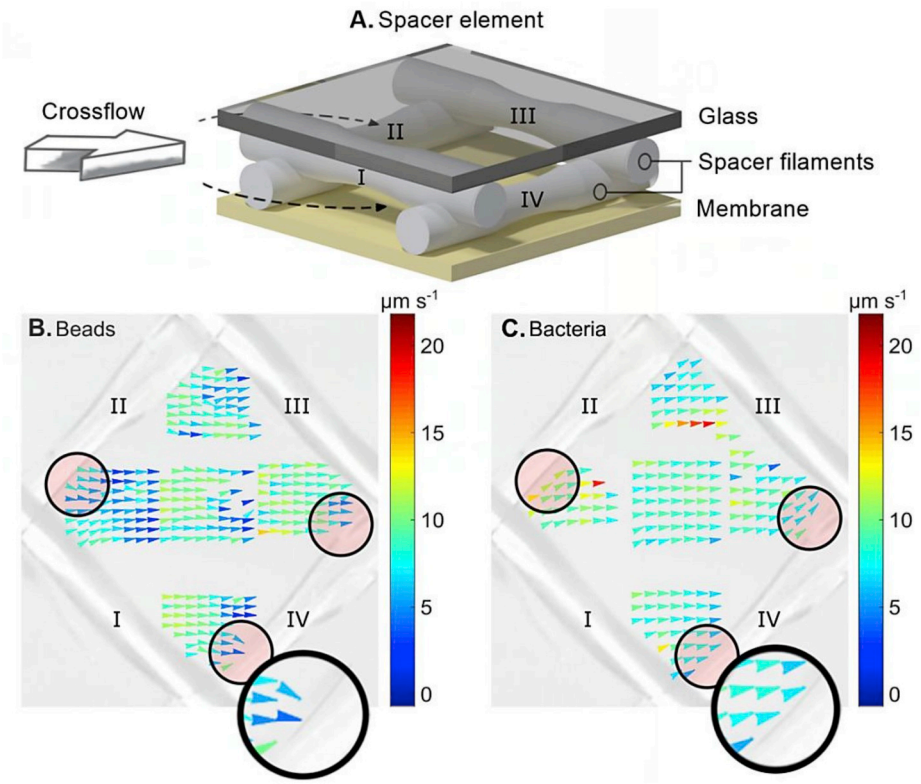

Fig. 3. Schematic illustration of the spacer configuration depicting the spacer filaments in contact with the glass (I, III) and in contact with the membrane (II, IV) (A). Direction and velocity of flow paths at the membrane surface within the area of one spacer element, derived from beads (B), and *B. subtilis* (C). Crossflow direction in the flow cell was kept constant from left to right. Arrows show the flow direction of the particles, while color coding indicates the velocity. Black circles highlight differences between beads and bacteria. Data was compiled out of three independent experiments for each foulant. (For interpretation of the references to color in this figure legend, the reader is referred to the Web version of this article.)

filaments, the contact with the membrane surface is not complete and gaps can occur [52,53].

Our results indicate that during the initial stages of cake formation, flow velocities close to the membrane surface (< 7 μm) were similar for beads and bacteria, reaching up to 17 μm s^{-1} (Fig. 3 B and C). In addition, flow paths of beads and bacteria had a similar flow direction (Fig. 3 B and C). Particles in the center of the spacer element were strongly influenced by the general crossflow, hence aligned with that overall direction. Previous studies have observed a similar alignment in flow fields obtained from particle image velocimetry using beads in spacer filled channels [25,51,54]. However, we deduce that the general flow direction was more dominant in this study since the applied crossflow velocity was lower (1 cm s^{-1}) than previously tested in the literature (7 cm s^{-1}) [25,51,54].

Although the general flow direction of beads and bacteria was similar, one important difference was observed in proximity to the spacer filaments in contact with the membrane (II and IV, Fig. 3 A). Bacteria and beads entered and left the spacer element by crossing under spacer filaments I and III in a perpendicular direction (Fig. 3 A and C). Additionally, flow paths obtained from beads also showed passage of beads underneath the filaments in contact with the membrane (II and IV, Fig. 3 A and B), confirming the presence of gaps between membrane and spacer filaments. Differently, spacer filaments in contact with the membrane formed a barrier to the flow of cells, since flow paths of bacteria in their proximity were parallel to the filament orientation (Fig. 3 C). Thus, beads closest to the membrane (< 7 μm) were able to pass underneath the filaments in contact with the membrane, while bacteria could not pass. This important difference suggests that the gap beneath the spacer filaments was immediately (< 5 min) clogged by the bacteria depositing from the feed solution. Only few bacteria cells that deposited on the membrane and attached beneath the filament may have been enough to congest the constricted space between spacer filament and membrane. We suggest that differently than the beads, the elongated shape (0.8 μm × 5 μm) of *B. subtilis* and extracellular polymeric substances (EPS) secreted by the cells had a critical impact on the initial clogging of the spacer element. Although the flow paths are mainly determined by the crossflow and spacer configuration, our results show that from the earliest stages of cake formation distinct differences are apparent between the flow paths of beads and bacteria. These differences can potentially affect the subsequent distribution of deposition and foulant accumulation. Yet, higher crossflow velocities (> 10 cm s^{-1}), which are used in full scale modules, may postpone the obstruction of the gap between membrane and spacer filaments due to higher shear at the membrane surface, thus reducing the differences between flow paths of beads and bacteria.

3.3. Spatiotemporal deposition patterns during the first and critical stages of cake formation

Quantification of deposition patterns during the initial stages of cake formation pointed to significant differences between beads and bacteria (Fig. 4). Our results indicate that the total amount of cells deposited on the membrane surface ($8.4 \pm 1.2 \times 10^3$ cells mm^{-2}) was nearly 3 fold higher than beads ($3.1 \pm 0.2 \times 10^3$ beads mm^{-2}) after 4 h of deposition. However, normalizing the final number of particles on the membrane surface to its initial concentration in the feed solution indicates that accumulation of bacteria was 20 times lower than that of the beads. Although differences in surface properties can strongly impact attachment efficiency, surface characteristics of the chosen beads and *B. subtilis* were similar (*i.e.* hydrophilic and negatively charged) [12,40,55]. Hence, we suggest that the initial attachment of *B. subtilis* was often reversed due to bacterial motility (Supporting information movie), thus reducing the accumulation of bacteria compared to the inert beads. Measured velocities of the flow field next to the membrane surface as obtained from the movement of particles were low (< 17 μm s^{-1}, Fig. 3 B). It should be noted that these velocities are well within the range of the propulsion of bacterial flagella (< 100 μm s^{-1}) and could thus be overcome by bacterial motility [10,56]. However, we suggest that bacterial motility may become too small to impact the deposition patterns as crossflow velocities are increased.

Supplementary video related to this article can be found at https://doi.org/10.1016/j.memsci.2019.117619

Starting with the inoculation of the feed solution, imaging of the membrane every 30 s facilitated the observation of differences in the deposition dynamics of beads and bacteria. Beads were deposited immediately after inoculation, while limited deposition of bacteria occurred during the first 2 h after inoculation on the unobstructed membrane area enclosed by the spacer element (Fig. 4 B and E). Analysis of the deposition rate indicated that beads followed a nearly linear slope (Fig. 4 B, $R^2 > 0.98$), while bacterial deposition increased exponentially (Fig. 4 E, $R^2 > 0.97$). We propose that the different trends were independent from the initial foulant concentration of the beads and bacteria. The linear deposition rate of the beads resulted from a constant concentration in the feed solution (Figs. S9 and S10), while the exponential

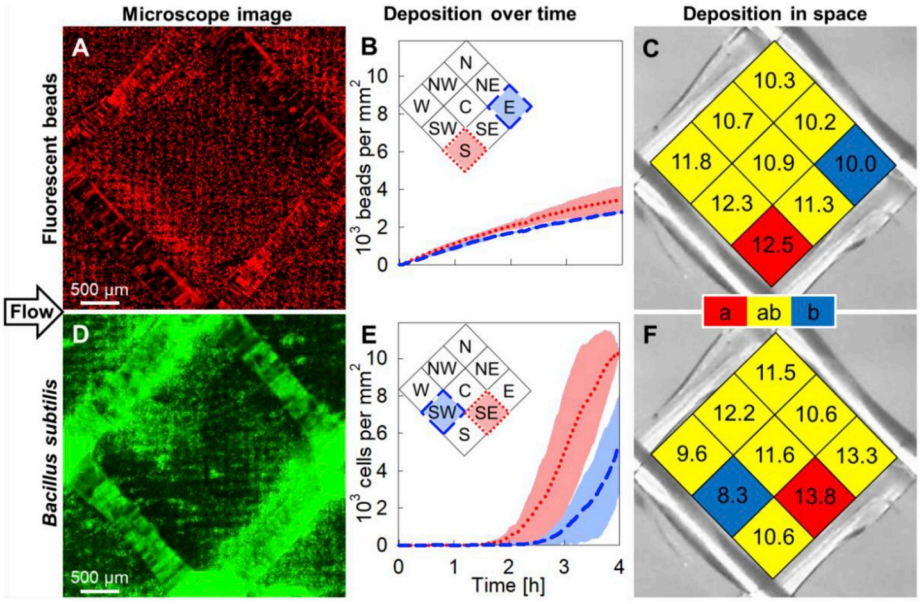

Fig. 4. Deposition of fluorescent beads and *B. subtilis* in FO experiments. The microscope images depict the deposition at the end of an experiment with beads in red (A) and *B. subtilis* in green (D). Deposition over time is shown for regions with highest (South-S in panel C, Southeast-SE in panel F) and lowest amount (East-E in panel C, Southwest-SW in panel F). The width of the shaded area is given by two standard deviations. Inserts in panels B and E indicate the denomination of the regions inside the spacer element according to the cardinal directions. Deposition in space was analyzed by calculating the partitioning between regions as the percentage of the total amount. Statistical analysis with ANOVA at a significance level of $p < 0.05$ resulted in two groups (a, b), which are represented by colors and are significantly different from each other (B and E). Data was collected and compared from three independent experiments for each foulant. (For interpretation of the references to color in this figure legend, the reader is referred to the Web version of this article.)

deposition rate of bacteria was due to bacterial growth in the feed solution (Figs. S9 and S10) and proliferation of bacteria on the membrane surface. An increase in bacteria concentration in the feed leads to an increase in cells transported towards the membrane surface, thus increasing deposition. However, the increase in bacteria concentration in the feed solution between 2 h and 4 h of the experiment was 5 fold, while the bacteria count on the membrane increased by 40 fold. Hence, we deduce that bacterial proliferation on the membrane surface had a greater impact on the amount of bacteria attached to the membrane than higher deposition rates. Therefore, we surmise that bacterial growth on the membrane and spacer surface is another key factor that differs between inert beads and live bacteria, especially for wastewater with high concentrations of nutrients and carbon sources.

Partitioning between regions within the spacer element displayed a significantly higher accumulation of beads in the South (S), while the East (E) showed the lowest deposition (Fig. 4 C). The ratio between these regions (S/E) resulted in a value of 1.25. Bacteria were deposited mostly in the Southeast (SE) and East (E) (Fig. 4 F), and in contrast to beads, the Southwest (SW) had the lowest deposition for bacteria (SE/SW = 1.66). According to the ratio between the regions with the highest and lowest amount, deposition within a spacer element was more homogenous for beads than bacteria.

The deposition pattern of the beads (Fig. 4 A and C) suggests that the decelerating flow downstream of the spacer filaments in contact with the glass (I, Fig. 3 A) enhanced deposition. Concomitantly, acceleration upstream of these filaments reduced deposition (III, Fig. 3 A). Previous studies pointed to a link between overall crossflow velocities and the deposition patterns in a spacer element [14,25,51]. Our results indicate that compared to a crossflow velocity of 7 cm s^{-1} [14], the lower crossflow velocities (1 cm s^{-1}) led to a deceleration of the flow with the entrained particles closer to the spacer filaments I and III after foulants passed under it. We suggest that a decrease in local velocities resulted in lower shear stress on the membrane, therefore deposition may move closer to the spacer filament.

Differently than beads, bacteria displayed a deposition minimum downstream of spacer filament I (Fig. 4 D and F). Irreversible attachment of bacteria on membrane and spacer surface is followed by the secretion of EPS and cell growth. Accumulation of EPS leads to significant blockage of feed solution flow, for example, in the gap between filament II or IV and the membrane. This blockage was already observed within the first minutes after inoculation via movies that determined bacteria flow paths (Fig. 3 C). Although very few bacteria deposited during the first 2 h, faster accumulation may have occurred underneath spacer filaments II and IV, which was excluded from the analyzed area. Additionally, very few bacteria and EPS could have been enough to clog this narrow gap (< 7 μm). Since the overall flow rate was kept constant throughout the experiment, there was an increase in local velocities in the unobstructed areas, which led to less deposition downstream of spacer filament I. Thus, the presence of EPS may have significantly influenced the spatial deposition pattern by changing the flow paths of bacteria compared to the inert beads. We suggest that these changes in flow velocities and direction during the early stages of biofilm formation would be more prominent than for beads due to the high proliferation rates of deposited bacteria.

3.4. Impact of beads and bacteria characteristics on deposition patterns during the early stages of cake formation

Here we provide a detailed comparison of the deposition patterns and flow paths of bacteria and beads during the initial stages of cake formation in a FO system with spacers under enhanced fouling conditions. The direction of flow paths obtained from inert beads and *B. subtilis* cells at the membrane surface during these early accumulation stages were highly similar. Hence, we surmise that the flow paths gained from beads provide a reliable approximation for the movement of bacteria (with similar size and shape) passing through a spacer element in a FO feed channel. However, our results also demonstrated important differences: (i) Passage of bacteria underneath the spacer filaments in contact with the membrane was impeded, while beads often passed freely (Fig. 3). These different flow paths may have contributed to the clear differences in spatiotemporal deposition of beads and bacteria (Fig. 4). (ii) Bacteria are living particles compared to inert beads, thus change the deposition patterns due to growth in the feed solution as well as on the surfaces of membranes and spacers. We deduce that during the initial stages of biofilm formation the proliferation of bacteria on the membrane surface would have a greater effect on biofouling development than physical deposition. (iii) Finally, velocities of flow fields near membranes and spacer surfaces are in the magnitude of motile bacteria. Hence, deposition patterns may also be impacted by the ability of bacteria to swim independently and actively detach from the surface.

Following the above, we surmise that the deposition of inert beads was mostly dictated by the flow regime, while the ability of bacterial cells to grow and move altered their deposition patterns. However, it should be noted that deposition patterns and quantities of inert beads as well as bacteria are likely to change under different operating conditions. Specifically, we suggest that future studies will use this methodological approach to study higher crossflow velocities and permeate water fluxes that are currently used in full scale facilities. It is possible that under these conditions bacteria may not be able to overcome the physical forces and act more similarly to inert beads. Additionally, this approach allows the investigation of other factors that may enhance or reduce the differences between beads and live bacteria, such as initial foulant concentrations, nutrient availability or bacterial motility. Nonetheless, the new imaging approach that was developed in this study and the corresponding results provide new insights on the biophysical aspects that control the early stages of cake formation. These initial stages are relevant in newly operated membrane modules or following cleaning of membrane systems with spacers and critical to the development of fouling. In addition, we surmise that the gained knowledge could be applicable to design new membrane surfaces and spacer shapes that minimize and delay fouling formation.

Author contributions

The manuscript was written through contributions of all authors. All authors have given approval to the final version of the manuscript.

Declaration of competing interest

There is no conflict of interest and all co-authors have seen and approved the current version for submission.

Acknowledgment

We thank James Kidwell of Conwed Plastics LLC, USA, and Porifera, USA for providing spacer samples and FO membranes, respectively, as well as Avigdor Eldar for sending us the GFP-labeled *B. subtilis* strain. We gratefully acknowledge the Kreitman School for Advanced Graduate studies of Ben-Gurion University of the Negev, Israel, for their support through the "Negev Tsin Scholarship" granted to Anne Bogler, as well as the Rieger Foundation and the Jewish National Fund for Anne's selection as a Rieger Foundation-Jewish National Fund Fellow in Environmental Studies in the 2018–2019 school year. This study was also supported by the BMBF-MOST Young Scientist Exchange Program, YSEP133, awarded to Andreas Kastl. This paper is in partial fulfillment of the Ph.D. thesis by Anne Bogler at Ben-Gurion University of the Negev.

Appendix A. Supplementary data

Supplementary data to this article can be found online at https://doi.org/10.1016/j.memsci.2019.117619.

References

[1] B.D. Coday, P. Xu, E.G. Beaudry, J. Herron, K. Lampi, N.T. Hancock, T.Y. Cath, The sweet spot of forward osmosis: treatment of produced water, drilling wastewater, and other complex and difficult liquid streams, Desalination 333 (2014) 23–35.

[2] K. Lutchmiah, A.R.D. Verliefde, K. Roest, L.C. Rietveld, E.R. Cornelissen, Forward osmosis for application in wastewater treatment: a review, Water Res. 58 (2014) 179–197.

[3] T.Y. Cath, A.E. Childress, M. Elimelech, Forward osmosis: principles, applications, and recent developments, J. Membr. Sci. 281 (2006) 70–87.

[4] J.R. McCutcheon, M. Elimelech, Influence of concentrative and dilutive internal concentration polarization on flux behavior in forward osmosis, J. Membr. Sci. 284 (2006) 237–247.

[5] R. Valladares Linares, S.S. Bucs, Z. Li, M. AbuGhdeeb, G. Amy, J.S. Vrouwenvelder, Impact of spacer thickness on biofouling in forward osmosis, Water Res. 57 (2014) 223–233.

[6] Y.C. Kim, S.J. Park, Experimental study of a 4040 spiral-wound forward-osmosis membrane module, Environ. Sci. Technol. 45 (2011) 7737–7745.

[7] H.-C. Flemming, G. Schaule, T. Griebe, J. Schmitt, A. Tamachkiarowa, Biofouling - the Achilles heel of membrane processes, Desalination 113 (1997) 215–225.

[8] A. Bogler, S. Lin, E. Bar-Zeev, Biofouling of membrane distillation, forward osmosis and pressure retarded osmosis: principles, impacts and future directions, J. Membr. Sci. 542 (2017) 378–398.

[9] E. Bar-Zeev, I. Berman-Frank, O. Girshevitz, T. Berman, Revised paradigm of aquatic biofilm formation facilitated by microgel transparent exopolymer particles, Proc. Natl. Acad. Sci. U.S.A. 109 (2012) 9119–9124.

[10] D. DeBeer, P. Stoodley, Microbial biofilms, in: E. Rosenberg, E.F. DeLong, E. Stackebrandt, S. Lory, F. Thompson (Eds.), Prokaryotes Appl. Bacteriol. Biotechnol, fourth ed., Springer, Berlin, 2013.

[11] S. Zou, Y.-N. Wang, F. Wicaksana, T. Aung, P.C.Y. Wong, A.G. Fane, C.Y. Tang, Direct microscopic observation of forward osmosis membrane fouling by microalgae: critical flux and the role of operational conditions, J. Membr. Sci. 436 (2013) 174–185.

[12] A. Subramani, E.M.V. Hoek, Direct observation of initial microbial deposition onto reverse osmosis and nanofiltration membranes, J. Membr. Sci. 319 (2008) 111–125.

[13] H. Li, A.G.G. Fane, H.G.L.G.L. Coster, S. Vigneswaran, Observation of particle deposition and removal behaviour of submicron bacteria on the membrane surface during crossflow microfiltration, J. Membr. Sci. 217 (2003) 29–41.

[14] A.I. Radu, M.S.H. van Steen, J.S. Vrouwenvelder, M.C.M. van Loosdrecht, C. Picioreanu, Spacer geometry and particle deposition in spiral wound membrane feed channels, Water Res. 64 (2014) 160–176.

[15] P.R. Neal, H. Li, A.G. Fane, D.E. Wiley, The effect of filament orientation on critical flux and particle deposition in spacer-filled channels, J. Membr. Sci. 214 (2003) 165–178.

[16] S. West, M. Wagner, C. Engelke, H. Horn, Optical coherence tomography for the in situ three-dimensional visualization and quantification of feed spacer channel fouling in reverse osmosis membrane modules, J. Membr. Sci. 498 (2016) 345–352.

[17] L. Fortunato, S. Bucs, R.V. Linares, C. Cali, J.S. Vrouwenvelder, T. Leiknes, Spatially-resolved in-situ quantification of biofouling using optical coherence tomography (OCT) and 3D image analysis in a spacer filled channel, J. Membr. Sci. 524 (2017) 673–681.

[18] L. Fortunato, Y. Jang, J.-G. Lee, S. Jeong, S. Lee, T. Leiknes, N. Ghaffour, Fouling development in direct contact membrane distillation: non-invasive monitoring and destructive analysis, Water Res. 132 (2018) 34–41.

[19] A.K. Prasad, Particle image velocimetry, Curr. Sci. 79 (2000) 51–60.

[20] R.J. Adrian, J. Westerweel, Particle image velocimetry, first ed., Cambridge University Press, 2011. New York.

[21] C. Dreszer, H.-C. Flemming, A.D. Wexler, A. Zwijnenburg, J.C. Kruithof, J. S. Vrouwenvelder, Development and testing of a transparent membrane biofouling monitor, Desalin. Water Treat. 52 (2014) 1807–1819.

[22] S. Kerdi, A. Qamar, J.S. Vrouwenvelder, N. Ghaffour, Fouling resilient perforated feed spacers for membrane filtration, Water Res. 140 (2018) 211–219.

[23] N. Thomas, N. Sreedhar, O. Al-Ketan, R. Rowshan, R.K. Abu Al-Rub, H. Arafat, 3D printed spacers based on TPMS architectures for scaling control in membrane distillation, J. Membr. Sci. 581 (2019) 38–49.

[24] M.R. Chowdhury, J. Steffes, B.D. Huey, J.R. McCutcheon, 3D printed polyamide membranes for desalination, Science 361 (2018) 682–686, 80-.

[25] S.S. Bucs, R.V. Linares, J.O. Marston, A.I. Radu, J.S. Vrouwenvelder, C. Picioreanu, Experimental and numerical characterization of the water flow in spacer-filled channels of spiral-wound membranes, Water Res. 87 (2015) 299–310.

[26] M.M. Motsa, B.B. Mamba, A. D'Haese, E.M.V. Hoek, A.R.D. Verliefde, Organic fouling in forward osmosis membranes: the role of feed solution chemistry and membrane structural properties, J. Membr. Sci. 460 (2014) 99–109.

[27] M. Xie, L.D. Nghiem, W.E. Price, M. Elimelech, A forward osmosis – membrane distillation hybrid process for direct sewer mining: system performance and limitations, Environ. Sci. Technol. 47 (2013) 13486–13493.

[28] E.A. Bell, R.W. Holloway, T.Y. Cath, Evaluation of forward osmosis membrane performance and fouling during long-term osmotic membrane bioreactor study, J. Membr. Sci. 517 (2016) 1–13.

[29] Y. Huang, M.C. Leu, J. Mazumder, A. Donmez, Additive Manufacturing: current state, future potential, gaps and needs, and recommendations, J. Manuf. Sci. Eng. 137 (2015) 1–10.

[30] W.S. Tan, S.R. Suwarno, J. An, C.K. Chua, A.G. Fane, T.H. Chong, Comparison of solid, liquid and powder forms of 3D printing techniques in membrane spacer fabrication, J. Membr. Sci. 537 (2017) 283–296.

[31] J.-Y. Lee, W.S. Tan, J. An, C.K. Chua, C.Y. Tang, A.G. Fane, T.H. Chong, The potential to enhance membrane module design with 3D printing technology, J. Membr. Sci. 499 (2016) 480–490.

[32] S.S. Giri, M. Harshiny, S.S. Sen, V. Sukumaran, S.C. Park, Production and characterization of a thermostable bioflocculant from *Bacillus subtilis* F9, isolated from wastewater sludge, Ecotoxicol. Environ. Saf. 121 (2015) 45–50.

[33] K. Chen, S. Xie, E. Iglesia, A.T. Bell, A PCR test to identify *Bacillus subtilis* and closely related species and its application to the monitoring of wastewater biotreatment, Appl. Microbiol. Biotechnol. 56 (2001) 816–819.

[34] J.N. Wilking, T.E. Angelini, A. Seminara, M.P. Brenner, D.A. Weitz, Biofilms as complex fluids, Mater. Res. Soc. Bull. 36 (2011) 385–392.

[35] X. Liu, L.-X. Foo, Y. Li, J.-Y. Lee, B. Cao, C.Y. Tang, Fabrication and characterization of nanocomposite pressure retarded osmosis (PRO) membranes with excellent anti-biofouling property and enhanced water permeability, Desalination 389 (2016) 137–148.

[36] J.N. Wilking, V. Zaburdaev, M. De Volder, R. Losick, M.P. Brenner, D.A. Weitz, Liquid transport facilitated by channels in *Bacillus subtilis* biofilms, Proc. Natl. Acad. Sci. 110 (2013) 848–852.

[37] E. Bar-Zeev, M. Elimelech, Reverse osmosis biofilm dispersal by osmotic back-flushing: cleaning via substratum perforation, Environ. Sci. Technol. Lett. 1 (2014) 162–166.

[38] Y. Sun, J. Tian, Z. Zhao, W. Shi, D. Liu, F. Cui, Membrane fouling of forward osmosis (FO) membrane for municipal wastewater treatment: a comparison between direct FO and OMBR, Water Res. 104 (2016) 330–339.

[39] E. Bar-Zeev, F. Perreault, A.P. Straub, M. Elimelech, Impaired performance of pressure-retarded osmosis due to irreversible biofouling, Environ. Sci. Technol. 49 (2015) 13050–13058.

[40] Ultrasensitive detection technology, in: I. Johnson, M.T.Z. Spence (Eds.), Mol. Probes Handb. A Guid. To Fluoresc. Probes Labeling Technol, eleventh ed., 2010.

[41] P. Glueckstern, M. Priel, E. Gelman, N. Perlov, Wastewater desalination in Israel, Desalination 222 (2008) 151–164.

[42] A. Bogler, D. Rice, F. Perreault, E. Bar-Zeev, Comparing membrane and spacer biofouling by Gram-negative *Pseudomonas aeruginosa* and Gram-positive *Anoxybacillus* sp. in forward osmosis, Biofouling J. Bioadhesion Biofilm Res. 35 (2019) 104–116.

[43] S. Lee, C. Boo, M. Elimelech, S. Hong, Comparison of fouling behavior in forward osmosis (FO) and reverse osmosis (RO), J. Membr. Sci. 365 (2010) 34–39.

[44] H. Yoon, Y. Baek, J. Yu, J. Yoon, Biofouling occurrence process and its control in the forward osmosis, Desalination 325 (2013) 30–36.

[45] Y. Wibisono, K.E. El Obied, E.R. Cornelissen, A.J.B. Kemperman, K. Nijmeijer, Biofouling removal in spiral-wound nanofiltration elements using two-phase flow cleaning, J. Membr. Sci. 475 (2015) 131–146.

[46] M. Modek Gimmelshtein, R. Semiat, Investigation of flow next to membrane walls, J. Membr. Sci. 264 (2005) 137–150.

[47] A.H. Haidari, S.G.J. Heijman, W.G.J. van der Meer, Visualization of hydraulic conditions inside the feed channel of reverse osmosis: a practical comparison of velocity between empty and spacer-filled channel, Water Res. 106 (2016) 232–241.

[48] T.R.R. Pintelon, S.A. Creber, D.A. Graf von der Schulenburg, M.L. Johns, Validation of 3D simulations of reverse osmosis membrane biofouling, Biotechnol. Bioeng. 106 (2010) 677–689.

[49] B. Manz, F. Volke, D. Goll, H. Horn, Measuring local flow velocities and biofilm structure in biofilm systems with Magnetic Resonance Imaging (MRI), Biotechnol. Bioeng. 84 (2003) 424–432.

[50] Y. Gao, S. Haavisto, C.Y. Tang, J. Salmela, W. Li, Characterization of fluid dynamics in spacer-filled channels for membrane filtration using Doppler optical coherence tomography, J. Membr. Sci. 448 (2013) 198–208.

[51] A.H. Haidari, S.G.J. Heijman, W.G.J. van der Meer, Effect of spacer configuration on hydraulic conditions using PIV, Separ. Purif. Technol. 199 (2018) 9–19.

[52] N. Horstmeyer, T. Lippert, D. Schön, F. Schlederer, C. Picioreanu, K. Achterhold, F. Pfeiffer, J.E. Drewes, CT scanning of membrane feed spacers – impact of spacer model accuracy on hydrodynamic and solute transport modeling in membrane feed channels, J. Membr. Sci. 564 (2018) 133–145.

[53] C. Picioreanu, J.S. Vrouwenvelder, M.C.M. van Loosdrecht, Three-dimensional modeling of biofouling and fluid dynamics in feed spacer channels of membrane devices, J. Membr. Sci. 345 (2009) 340–354.

[54] P. Willems, N.G. Deen, A.J.B. Kemperman, R.G.H. Lammertink, M. Wessling, M. van Sint Annaland, J.A.M. Kuipers, W.G.J. van der Meer, Use of Particle Imaging Velocimetry to measure liquid velocity profiles in liquid and liquid/gas flows through spacer filled channels, J. Membr. Sci. 362 (2010) 143–153.

[55] J.M. Meinders, H.C. van der Mei, H.J. Busscher, Deposition efficiency and reversibility of bacterial adhesion under flow, J. Colloid Interface Sci. 176 (1995) 329–341.

[56] D. Giacché, T. Ishikawa, T. Yamaguchi, Hydrodynamic entrapment of bacteria swimming near a solid surface, Phys. Rev. E. 82 (2010) 1–8.